JOURNAL OF PROPULSION AND POWER
Vol. 21, No. 3, May–June 2005

Fuel-Cell-Powered Magnetoplasma Jet Engine with Electron Beam Ionization

Bernard Parent* and In-Seuck Jeung†
Seoul National University, Seoul 151-744, Republic of Korea

A fuel-cell-powered magnetoplasma jet engine (magjet) using electron-beam ionizers is here proposed for air-breathing flight in the supersonic/hypersonic regime. The engine consists of a fuel-cell duct containing the power source and of a high-speed duct producing most of the thrust through a magnetoplasmadynamic (MPD) accelerator. To reduce the shocks and heat loads in the fuel cells, the enthalpy of the air is extracted beforehand through a MPD generator. The power produced by the latter and by the fuel cells is then split optimally between the MPD accelerator located in the high-speed duct and one located downstream of the fuel cells. The performance is assessed through exact solutions of a quasi-one-dimensional model, which includes the effect of ion slip, Joule heating, and heat dissipated through electron-beam ionization. The magnetic field strength as well as the mass-flow-rate ratio between the high-speed and fuel-cell ducts are seen to affect the thrust considerably at lower Mach number, but to have a smaller impact at hypervelocities. Flight beyond Mach 6 would necessitate substantial cooling of the fuel cells caused by the ion slip effect preventing sufficient enthalpy extraction, independently of the magnetic field strength. For a fuel-cell efficiency of 0.6 and a mass-flow-rate ratio of 5, the magjet delivers a specific impulse within 15% of the one of the turbojet in the Mach number range 1–3 given a magnetic field of 8 T. From Mach 3 to 5, a magnetic field strength varying between 2 and 4 T is seen to be sufficient to match the performance of conventional engines.

Nomenclature

A	=	cross-sectional area
$\mathcal{A}$	=	Avogadro's number, 6.02257×10^{23}
a	=	speed of sound
$\boldsymbol{B}$	=	magnetic field vector
b	=	term function of ξ and γ, defined in Eq. (10)
C_p	=	specific heat at constant pressure
C_v	=	specific heat at constant volume
$\boldsymbol{E}$	=	electric field vector
e	=	charge of one electron, 1.60207×10^{-19} C
e_f	=	specific energy of the fuel, J/kg
F	=	thrust
g	=	gravitational acceleration, 9.81 kgm/s^2
H	=	total enthalpy, $h + q^2/2$
h	=	enthalpy, $C_P T$
I_{sp}	=	specific impulse
J	=	term related to the heat addition, defined in Eq. (5)
$\boldsymbol{j}$	=	current density vector
k	=	electromagnetic load factor, $\boldsymbol{E}_y/q\boldsymbol{B}_z$
k_c	=	electron scattering rate constant
k_{dr}	=	rate constant of dissociative recombination
M	=	Mach number
$\mathcal{M}_a$	=	molecular weight of air, 0.029 kg
m_e	=	mass of one electron, 9.1095×10^{-31} kg
m_n	=	mass of a neutral molecule (for air, 4.815×10^{-26} kg)
$\dot{m}$	=	mass flow rate
$\dot{m}_{\text{fuel}}$	=	fuel mass flow rate in the fuel cells
n_e	=	electron number density
n_n	=	concentration of neutral components
P	=	pressure
$\mathcal{P}_1$	=	power output from MPD generator in fuel cell duct
$\mathcal{P}_2$	=	power generated by fuel cells
$\mathcal{P}_3$	=	power input to the MPD accelerator in high speed duct
$\mathcal{P}_4$	=	power input to the MPD accelerator in fuel cell duct
$\mathcal{P}_5$	=	excess heat generated by the fuel cells and distributed to the air
P_{dyn}	=	flight dynamic pressure, $\rho_1 q_1^2/2$
Q_i	=	heat addition originating from electron-beam ionization
q	=	flow speed
T	=	temperature
$\boldsymbol{v}$	=	velocity vector
x	=	engine streamwise coordinate
Y_i	=	energy cost of an ion-electron pair using electron-beam ionization, 35 eV, 5.61×10^{-18} J
β_e	=	Hall parameter for the electrons, $\beta'_e\lvert\boldsymbol{B}\rvert/\rho$
β'_e	=	term related to the Hall parameter for the electrons, $\sim$0.1
β_i	=	Hall parameter for the ions, $\beta'_i\lvert\boldsymbol{B}\rvert/\rho$
β'_i	=	term related to the Hall parameter for the ions, $\beta'_e\sqrt{(m_e/m_n)}$
γ	=	ratio of specific heats, C_p/C_v
η_e	=	engine efficiency
η_{fc}	=	fuel cell efficiency
ξ	=	ratio between the heat and work terms part of the energy transport equation
ξ_a	=	magnitude of ξ in high-speed duct
ξ_b	=	magnitude of ξ in fuel cell duct
ρ	=	density
σ	=	electrical conductivity
σ_e	=	effective electrical conductivity, $\sigma/(1+\beta_e\beta_i)$
Φ	=	fraction of the power generated by fuel cells and extracted from the incoming flow, which is bypassed to the high-speed duct
ϕ_s	=	stoichiometric mass fraction between fuel and air

Subscripts

a	=	high-speed duct

Received 8 October 2003; revision received 20 September 2004; accepted for publication 25 October 2004.

*Research Associate, School of Mechanical and Aerospace Engineering; currently Visiting Research Fellow, Dept. of Mechanical and Aerospace Engineering, Princeton University, Princeton, NJ 08544; bernard@snu.ac.kr.

†Professor, School of Mechanical and Aerospace Engineering; also with Institute of Advanced Aerospace Technology; enjis@snu.ac.kr. Associate Fellow AIAA.

b	=	fuel-cell duct
opt	=	optimal
x, y, z	=	vector components along Cartesian coordinates
1	=	freestream conditions
$1a, 2a, 6a$	=	x stations in high-speed duct
$1b, 2b, 3b, 4b, 6b$	=	x stations in fuel-cell duct

Superscript

$\circ$	=	stagnation

Introduction

AIRBREATHING jet engines propulsing present-day aircraft provide thrust through conversion of the heat added chemically into work, which is accomplished by compressing and expanding the fluid before and after the heat addition, respectively. Although this has proven to be a viable concept for flight over a limited Mach-number range, extending the flight Mach-number envelope of airbreathing jet engines is not a trivial task. Difficulties originate from the complicated compression process in the inlet, which needs to be accomplished with minimal losses. To minimize losses while maintaining a high pressure in the combustor, radical variations in the design/geometry of the engine are needed as the aircraft accelerates from rest to hypersonic speeds.

This prompted the development of substantially different engine designs such as the turbojet, the ramjet, and the scramjet to cover the flight Mach number envelopes 0–3, 3–7, and 7–15, respectively. It follows that to operate from rest to high speeds the different designs must be combined into one or somehow substituted to one another during flight. Adding to the challenge are the high heat loads characteristic of hypersonic flight effectively rendering any type of mechanical control on the engine geometry a challenging endeavor.

To circumvent these difficulties, a novel propulsion concept dubbed the magnetoplasma jet engine, or magjet, is here proposed. Contrary to conventional engines which are characterized by energy addition to the flow as heat, the magjet is advantaged by electromagnetic energy addition to the flow mostly as work, with the power source being a stack of fuel cells. By not requiring the flow to be compressed and expanded, the magjet can operate with little variations in geometry.

To prevent the occurrence of shocks and high heat loads in the fuel-cell compartment, the enthalpy is extracted electromagnetically such that the Mach number of the air does not exceed one at the entrance of the fuel cell compartment (see Fig. 1). Flow deceleration through electromagnetic energy extraction[1–8] can result in a lower temperature increase than would be obtained through standard gasdynamic deceleration. Further, it can be achieved in a constant-area duct, hence not requiring significant variations in geometry as the flight Mach number varies. To minimize performance penalties originating from the enthalpy extraction process, the amount of air decelerated electromagnetically is limited to the minimal value needed for the fuel cells to operate.

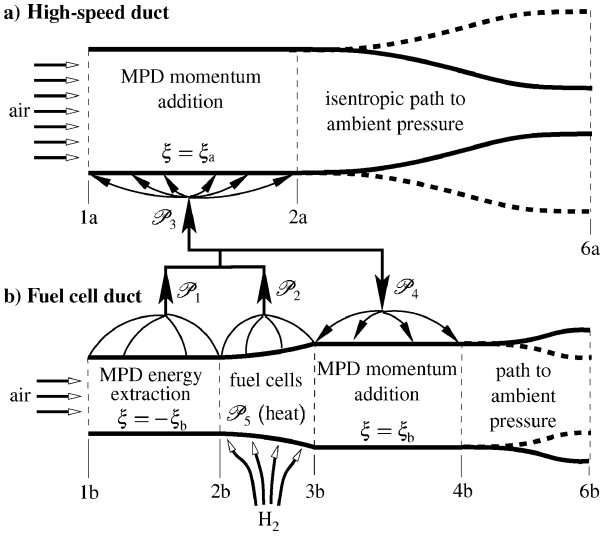

Fig. 1 Schematic of the fuel-cell-powered magjet.

The power generated through enthalpy extraction is combined with the power produced by the fuel cells and is then deposited to the flow mostly as work through electromagnetic momentum addition processes, hence producing thrust. A portion of the power is deposited to the flow exiting the fuel cells, and the remaining power is deposited to the flow in the high-speed duct. The amount of power bypassed to the high-speed duct is such that the thrust is maximized.

One objective of this paper is to quantify the effect of the magnetic field strength and of the mass flow rate ratio between the high-speed and fuel-cell ducts on the performance of the engine. A second objective is to assess the Mach-number range in which the magjet can yield gains in specific impulse compared to the turbojet or ramjet. A third objective is to determine the maximum flight Mach number for which the stagnation temperature in the fuel-cell compartment can be kept to a reasonably low value.

The results are obtained through exact solutions of a quasi-one-dimensional model of the Euler equations including the electromagnetic source terms, the heat dissipated through electron-beam ionization, and the Hall/ion-slip effects. In assessing the performance, it is assumed that the energy conversion efficiency of the fuel cells is of 0.6. Although future fuel cells are expected to reach an efficiency approaching 0.7–0.8 (Ref. 9), it is here preferred to use a value closer to the 0.4–0.5 efficiency exhibited by current fuel cells intended for transportation purposes.[10,11]

Governing Equations

The steady-state quasi-one-dimensional flow equations for a calorically and thermally perfect gas including the electromagnetic source terms and the heat generated through electron-beam ionization can be written as follows:

Continuity:

$$\frac{\mathrm{d}}{\mathrm{d}x} A\rho q = 0 \tag{1}$$

Momentum:

$$\rho q \frac{\mathrm{d}q}{\mathrm{d}x} + \frac{\mathrm{d}P}{\mathrm{d}x} = (\boldsymbol{j} \times \boldsymbol{B})_x \tag{2}$$

Energy:

$$\rho q \frac{\mathrm{d}}{\mathrm{d}x}\left(h + \frac{1}{2}q^2\right) = \frac{\boldsymbol{j}\cdot\boldsymbol{j}}{\sigma_e} + Q_i + q(\boldsymbol{j} \times \boldsymbol{B})_x \tag{3}$$

The gas is assumed thermally and calorically perfect, and the current density is obtained from the electric and magnetic fields according to Ohm's law:

$$\boldsymbol{E} = \boldsymbol{j}/\sigma_e + \boldsymbol{B} \times \boldsymbol{v} \tag{4}$$

For simplicity, the electromagnetic Joule heating term $\boldsymbol{j}\cdot\boldsymbol{j}/\sigma_e$ and work interaction term $q(\boldsymbol{j} \times \boldsymbol{B})_x$ shall be referred to in this paper as the Joule heating and work interaction terms, respectively. The sum between the Joule heating and the energy per unit volume added through electron-beam ionization Q_i shall be referred to as the heat addition.

Exact Solutions

A brief outline of some exact solutions applicable to the governing equations under consideration is here given. For a complete derivation, the reader can consult Ref. 12.

By defining J as follows

$$\mathrm{d}J \equiv \frac{\gamma - 1}{\gamma} \frac{\boldsymbol{j}\cdot\boldsymbol{j} + \sigma_e Q_i}{Pq\sigma_e}\,\mathrm{d}x \tag{5}$$

the pressure and Mach number ratios take the form:

$$P_2/P_1 = (T_2/T_1)^{\gamma/(\gamma-1)}[\exp(J_2 - J_1)]^{-\gamma/(\gamma-1)} \tag{6}$$

$$M_2/M_1 = (T_1/T_2)^{(\gamma+1)/2(\gamma-1)}[\exp(J_2 - J_1)]^{\gamma/(\gamma-1)} \tag{7}$$

which hold true for a constant-γ path in which no entropy generating phenomenon is present other than those caused by electromagnetic Joule heating and to heat deposition from external ionization. Although the latter two equations can be used for constant-area flow, they are also applicable to a stream tube in which the area varies.

To express $\exp(J_2 - J_1)$ as a function of flow properties, we first define the heat/work ratio ξ as

$$\xi \equiv \frac{(\boldsymbol{j}\cdot\boldsymbol{j}/\sigma_e + Q_i)}{[\,q(\boldsymbol{j}\times\boldsymbol{B})_x]} \tag{8}$$

Then, as long as ξ, γ, and the cross-sectional area are constant from station 1 to 2, it can be shown that

$$\exp(J_2 - J_1) = \frac{T_2^\circ}{T_1^\circ}\left(\frac{P_2^\circ}{P_1^\circ}\right)^{(1-\gamma)/\gamma} = \left(\frac{b - M_1^2}{b - M_2^2}\right)^{(b-1)/\gamma b}\left(\frac{M_1}{M_2}\right)^{2/\gamma b} \tag{9}$$

where b is a function of γ and ξ:

$$b = \frac{(\gamma+1)(\xi+1) - 2\gamma\xi}{\gamma\xi(\gamma-1)} \tag{10}$$

In applying Eq. (9), it is important to ensure that only physically meaningful solutions are obtained by verifying that the appropriate condition is satisfied among the following:

$$\begin{aligned}
&b < M_1^2 \quad \text{if} \quad M_2 > M_1 \quad \text{and} \quad M_1, M_2 \le 1\\
&b > M_1^2 \quad \text{if} \quad M_2 < M_1 \quad \text{and} \quad M_1, M_2 \le 1\\
&b > M_2^2 \quad \text{if} \quad M_2 > M_1 \quad \text{and} \quad M_1, M_2 \ge 1\\
&b < M_2^2 \quad \text{if} \quad M_2 < M_1 \quad \text{and} \quad M_1, M_2 \ge 1
\end{aligned} \tag{11}$$

Combining Eq. (7) with Eq. (9) and isolating T_2/T_1 yields the following relation for the temperature ratio in a constant-area duct:

$$\frac{T_2}{T_1} = \left(\frac{b - M_1^2}{b - M_2^2}\right)^{2(b-1)/b(\gamma+1)}\left(\frac{M_1}{M_2}\right)^{[(\gamma-1)2b+4]/b(\gamma+1)} \tag{12}$$

As schematized in Fig. 2, for a flow in a constant-area duct in which the electric field, magnetic field, and velocity vector are perpendicular to one another and where ξ, γ, and $\sigma_e \boldsymbol{B}_z^2(k-1)$ are constant, the following holds:

$$\frac{\sigma_e \boldsymbol{B}_z^2(x_2 - x_1)(k-1)}{\rho q} = \frac{b\gamma + 1}{b(\gamma+1)\gamma} \times \ell_n\left\{\left[\frac{M_2^2\left(b - M_1^2\right)}{M_1^2\left(b - M_2^2\right)}\right]^{(b-1)/b}\frac{\exp\left(M_2^{-2}\right)}{\exp\left(M_1^{-2}\right)}\right\} \tag{13}$$

where k is the work interaction parameter corresponding in this case to $\boldsymbol{E}_y/q\boldsymbol{B}_z$.

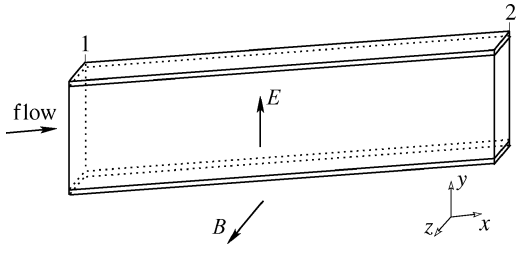

Fig. 2 Constant-area duct with perpendicular velocity, magnetic field, and electric field vectors.

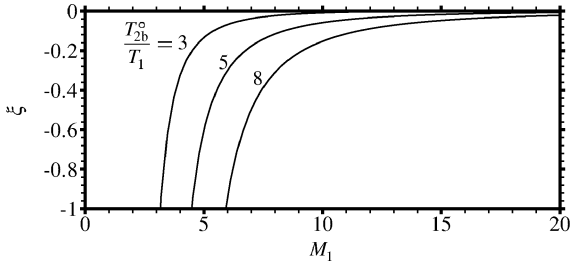

Fig. 3 Heat/work ratio in the energy extraction section as a function of the flight Mach number.

Energy Extraction

At high flight Mach number, it is important to extract sufficient enthalpy from the flow entering the fuel-cell duct: should the stagnation temperature of the air be too high, the fuel cells would require excessive cooling to operate. Because the amount of energy extracted is expected to be restrained by the amount of heat added, it is hence important to minimize the latter. In this section, we wish to find the maximum permissible value of the heat/work ratio in the magnetoplasmadynamic (MPD) generator that would yield an acceptable stagnation temperature in the fuel cells.

The ratio between the air stagnation temperature in the fuel cells and the freestream temperature can be found starting from Eq. (12) and using standard gasdynamic relationships:

$$\frac{T_{2b}^\circ}{T_1} = \left(1 + \frac{\gamma-1}{2}M_{2b}^2\right)\left(\frac{b - M_1^2}{b - M_{2b}^2}\right)^{2(b-1)/b(\gamma+1)} \times \left(\frac{M_1}{M_{2b}}\right)^{[(\gamma-1)2b+4]/b(\gamma+1)} \tag{14}$$

where γ and M_{2b} are set to 1.4 and 1, respectively. From the latter, b can be determined for a given intake Mach number and ratio between the stagnation temperature in the fuel-cell compartment and the freestream temperature. From b, the heat/work ratio ξ can be obtained from Eq. (10). The Mach number at the entrance of the fuel cells is fixed to 1, which corresponds to the choking point for MPD energy extraction in a constant-area duct.[13]

As Fig. 3 shows, a relatively high magnitude of the heat/work ratio in the range 0.2–1 is restrictive on the maximum flight Mach number attainable. Indeed, the maximal flight Mach number cannot exceed seven for a fuel-cell compartment entrance stagnation temperature five times the flow incoming temperature. Meanwhile, upon reducing the heat to 2% of the work, it is possible to attain a flight Mach number up to 15. However, as shall be seen in a subsequent section, reducing the heat/work ratio to that level would be very hard if not impossible to obtain in practice.

Thrust

High-Speed Duct

A general expression is here obtained for the force exerted by the fluid on the high-speed duct in the direction of motion F_a. Neglecting the viscous effects, assuming that the pressure is uniform and equal to ambient on the outer surface of the engine, and assuming that the pressure at the engine exit plane is equal to ambient, it can be shown that

$$F_a/\dot{m}_a q_{1a} = q_{6a}/q_{1a} - 1 \tag{15}$$

Also, the difference in total enthalpies between station 1a and 6a can be related to the power input as $H_{6a} - H_{1a} = \mathcal{P}_3/\dot{m}_a$, which, after some algebra, becomes

$$\frac{2}{(\gamma-1)M_{1a}^2}\left(\frac{T_{6a}}{T_{1a}} - 1\right) + \frac{q_{6a}^2}{q_{1a}^2} - 1 = \frac{2\mathcal{P}_3}{\dot{m}_a q_{1a}^2} \tag{16}$$

where the temperature ratio can be expressed as a function of $(J_{6a} - J_{1a})$ through Eq. (6) noting that the pressure ratio is one in this case. Then, q_{6a}/q_{1a} is isolated in the latter and is substituted back into Eq. (15) to yield

$$\frac{F_a}{\dot{m}_a q_{1a}} = \left\{ \frac{2\left[1 - \exp\left(J_{6a} - J_{1a}\right)\right]}{(\gamma - 1)M_{1a}^2} + 1 + \frac{2\mathcal{P}_3}{\dot{m}_a q_{1a}^2} \right\}^{\frac{1}{2}} - 1 \quad (17)$$

The normalized thrust of the high-speed duct is hence seen to be a function of the specific heat ratio, intake Mach number, normalized power input, and a term related to the amount of heat addition, $\exp(J_{6a} - J_{1a})$. The latter shall be determined in a following section.

Fuel-Cell Duct

Similarly to the determination of the thrust for the high-speed duct, F_b (the force exerted by the fluid on the fuel duct in the direction of motion) is determined assuming that the flow pressure is equal to ambient at the duct exit, and that the pressure on the outer surface is equal to the one in the freestream. Following a similar approach as in the preceding section, it can be shown that

$$\frac{F_b}{\dot{m}_b q_{1b}} = \left\{ \frac{2[1 - \exp(J_{6b} - J_{1b})]}{(\gamma - 1)M_{1b}^2} + 1 + \frac{2(\mathcal{P}_5 + \mathcal{P}_4 - \mathcal{P}_1)}{\dot{m}_b q_{1b}^2} \right\}^{\frac{1}{2}} - 1 \quad (18)$$

Combined Thrust

The overall thrust F corresponds to the sum of the thrust of the high-speed and fuel-cell ducts. Noting that the inflow properties are the same for both ducts and that $\mathcal{P}_3 = \Phi(\mathcal{P}_1 + \mathcal{P}_2)$ and $\mathcal{P}_4 = (1 - \Phi)(\mathcal{P}_1 + \mathcal{P}_2)$, the normalized thrust can be shown to correspond to

$$\frac{F}{\dot{m}_b q_1} = -1 - \frac{\dot{m}_a}{\dot{m}_b} + \left\{ \frac{2[1 - \exp(J_{6b} - J_{1b})]}{(\gamma - 1)M_1^2} + 1 + \frac{2[\mathcal{P}_5 + \mathcal{P}_2(1 - \Phi) - \Phi\mathcal{P}_1]}{\dot{m}_b q_1^2} \right\}^{\frac{1}{2}} + \frac{\dot{m}_a}{\dot{m}_b} \left\{ \frac{2[1 - \exp(J_{6a} - J_{1a})]}{(\gamma - 1)M_1^2} + 1 + \frac{\dot{m}_b}{\dot{m}_a} \frac{2\Phi(\mathcal{P}_1 + \mathcal{P}_2)}{\dot{m}_b q_1^2} \right\}^{\frac{1}{2}} \quad (19)$$

At this stage, the losses-related terms $\exp(J_{6a} - J_{1a})$ and $\exp(J_{6b} - J_{1b})$ need to be determined as a function of known parameters and flow properties.

Determination of $\exp(J_{6a} - J_{1a})$

Because electromagnetic control is only applied between stations $1a$ and $2a$ in the high-speed duct, the term $\exp(J_{6a} - J_{1a})$ corresponds to $\exp(J_{2a} - J_{1a})$, which can be obtained from Eq. (9), provided that M_{2a} is known. The Mach number at station $2a$ can be found noting that the total enthalpy change from station $1a$ to station $2a$ corresponds to the ratio between the power input and the mass flow rate, that is, $\dot{m}_a H_{2a} = \dot{m}_a H_{1a} + \mathcal{P}_3$. With the help of Eq. (12), and noting that $\mathcal{P}_3 = \Phi(\mathcal{P}_1 + \mathcal{P}_2)$, the following is obtained:

$$\left(\frac{b - M_{1a}^2}{b - M_{2a}^2}\right)^{2(b-1)/b(\gamma+1)} \left(\frac{M_{1a}}{M_{2a}}\right)^{[(\gamma-1)2b+4]/b(\gamma+1)} \times \left(1 + \frac{\gamma - 1}{2} M_{2a}^2\right) = 1 + \frac{\gamma - 1}{2} M_{1a}^2 \left[1 + \frac{\dot{m}_b}{\dot{m}_a} \frac{2\Phi(\mathcal{P}_1 + \mathcal{P}_2)}{\dot{m}_b q_{1b}^2}\right] \quad (20)$$

which yields the Mach number at station $2a$ for a given power generated by the fuel cells and the MPD generator located upstream of the fuel-cell compartment. Those shall be determined in a subsequent section as a function of the inflow conditions.

Determination of $\exp(J_{6b} - J_{1b})$

The term related to the heat addition and losses in the fuel-cell duct can be shown to correspond to

$$\exp(J_{6b} - J_{1b}) = \exp(J_{2b} - J_{1b}) \exp(J_{4b} - J_{3b}) \times \left(T_{3b}^{\circ} / T_{2b}^{\circ}\right)\left(P_{3b}^{\circ} / P_{2b}^{\circ}\right)^{(1-\gamma)/\gamma} \quad (21)$$

where the first two terms on the right-hand side (RHS) can be obtained from Eq. (9), provided that the Mach number is known at the entrance/exit of the fuel-cell compartment as well as at station $4b$. In this paper, the Mach number at the entrance and exit of the fuel-cell compartment is always fixed to one, and an expression yielding M_{4b} can be obtained similarly to the one yielding M_{2a} in the preceding section:

$$\left(\frac{b - M_{3b}^2}{b - M_{4b}^2}\right)^{2(b-1)/b(\gamma+1)} \left(\frac{M_{3b}}{M_{4b}}\right)^{[(\gamma-1)2b+4]/b(\gamma+1)} \times \left(1 + \frac{\gamma - 1}{2} M_{4b}^2\right) = 1 + \frac{\gamma - 1}{2} M_{3b}^2 \times \left[1 + \frac{M_{1b}^2}{M_{3b}^2} \frac{T_{1b}}{T_{2b}} \frac{T_{2b}}{T_{3b}} \frac{2(1 - \Phi)(\mathcal{P}_1 + \mathcal{P}_2)}{\dot{m}_b q_{1b}^2}\right] \quad (22)$$

where T_{2b}/T_{1b} can be expressed as a function of the Mach number at station $2b$ from Eq. (12) and where the temperature ratio across the fuel-cells can be expressed as a function of the stagnation temperature ratio $T_{3b}^{\circ}/T_{2b}^{\circ}$ from standard gasdynamic expressions. Equation (22) hence yields M_{4b} given the stagnation temperature ratio across the fuel-cells compartment as well as the normalized power generation terms.The latter are now determined.

Power Generation Terms

A relationship between the power extracted in the energy extraction section and the Mach number at its extrema can be obtained similarly to the expression shown in Eq. (20). Then, isolating the normalized power extracted, we get

$$\frac{\mathcal{P}_1}{\dot{m}_b q_{1b}^2} = \frac{1}{2} - \frac{1}{(\gamma - 1)M_{1b}^2}\left[-1 + \left(\frac{b - M_{1b}^2}{b - M_{2b}^2}\right)^{2(b-1)/b(\gamma+1)} \times \left(\frac{M_{1b}}{M_{2b}}\right)^{[(\gamma-1)2b+4]/b(\gamma+1)} \left(1 + \frac{\gamma - 1}{2} M_{2b}^2\right)\right] \quad (23)$$

with all of the terms on the RHS being user specified.

To determine the power generated by the fuel cells, it is assumed that the entire amount of oxygen flowing in the fuel-cell duct is used by the fuel cells to generate electricity. The power generated by the fuel cells would hence correspond to the product of the fuel-cell efficiency η_{fc} by the fuel specific energy e_f and by the mass flow rate of the fuel. Noting that $\dot{m}_{\text{fuel}} = \dot{m}_b \phi_s$, it follows that

$$\mathcal{P}_2 / \dot{m}_b q_{1b}^2 = \left(1 / M_{1b}^2\right)\left(\phi_s \eta_{\text{fc}} e_f / a_{1b}^2\right) \quad (24)$$

where ϕ_s is the stoichiometric mass fraction between the fuel and the air. Because hydrogen is the chosen fuel, ϕ_s and e_f are hereafter set to 0.03 and 142 MJ/kg (Ref. 14), respectively.

From the total enthalpy balance across the fuel-cell compartment, a relationship exists between $\mathcal{P}_5$ and the stagnation temperature ratio. Combined with Eq. (12), this would yield:

$$\frac{\mathcal{P}_5}{\dot{m}_b q_{1b}^2} = \frac{1}{M_{1b}^2}\left(\frac{b - M_{1b}^2}{b - M_{2b}^2}\right)^{2(b-1)/b(\gamma+1)} \left(\frac{M_{1b}}{M_{2b}}\right)^{[(\gamma-1)2b+4]/b(\gamma+1)} \times \left(\frac{1}{\gamma - 1} + \frac{M_{2b}^2}{2}\right)\left(\frac{T_{3b}^{\circ}}{T_{2b}^{\circ}} - 1\right) \quad (25)$$

Power Bypass Ratio

The ratio of the power bypassed to the high-speed duct Φ is determined such that the thrust is maximized. The optimal value for the power bypass ratio is hence a function of the same parameters the thrust is a function of, that is,

$$\Phi_{\text{opt}} = f_1\left(\gamma, \frac{\phi_s \eta_{\text{fc}} e_f}{a_1^2}, M_{2b}, M_{3b}, \frac{P_{3b}^\circ}{P_{2b}^\circ}, \frac{T_{3b}^\circ}{T_{2b}^\circ}, M_1, \xi_a, \xi_b, \frac{\dot{m}_a}{\dot{m}_b}\right) \quad (26)$$

where the Mach number at stations $2b$ and $3b$ is fixed to 1, the stagnation pressure and temperature ratios in the fuel compartment are set to 1, γ is set to 1.4, and $\phi_s \eta_{\text{fc}} e_f / a_1^2$ is set to 26.06.

In Fig. 4, it can be seen that an increase in the flight Mach number induces a considerable reduction in the power bypass ratio, especially when the mass flow rate ratio is high. This can be explained as follows: because the thrust is sensitive to the mass flow rate for a small intake Mach number, a high mass flow rate ratio induces a significant fraction of the power bypassed to the high-speed duct at low speed. On the other hand, at higher flight speed it becomes more efficient to add more power to the slow speed flow exiting the fuel-cell compartment, as a result of the thrust becoming progressively more sensitive to the flow speed rather than the mass flow rate.

Keeping the mass flow rate ratio constant, Fig. 4b shows the impact of the heat/work ratio on the power bypassed. It is apparent that an increase in the value of the heat/work ratio in the high-speed duct translates into a decrease of power delivered to the latter. Similarly, an increase in the heat/work ratio in the fuel-cell duct results into less power transferred to that part of the engine. This is to be expected as an increase in the heat addition necessarily translates into a smaller amount of power being converted into work: to maximize the work, it is hence more efficient to raise the amount of power delivered to the duct where less heat is generated. Indeed, because the flow is not compressed significantly prior to the energy addition most of the heat added does not get converted into work and hence thrust.

Efficiency

The engine efficiency is here defined as the ratio between the thrust of the engine multiplied by the flight speed and the power generated by the fuel cells, that is, $\eta_e \equiv Fq_1/\mathcal{P}_2$ with the thrust obtained from Eq. (19). The engine efficiency is seen to be a function of

$$\eta_e = f_2\left(\gamma, \frac{\phi_s \eta_{\text{fc}} e_f}{a_1^2}, M_{2b}, M_{3b}, \frac{P_{3b}^\circ}{P_{2b}^\circ}, \frac{T_{3b}^\circ}{T_{2b}^\circ}, M_1, \xi_a, \xi_b, \frac{\dot{m}_a}{\dot{m}_b}\right) \quad (27)$$

where the Mach number at the entrance/exit of the fuel-cell compartment is fixed to 1, the stagnation pressure/temperature ratios are set to 1, the specific heat ratio is set to 1.4, and the term $\phi_s \eta_{\text{fc}} e_f / a_1^2$ is given a value of 26.06.

A high mass flow rate ratio is seen in Fig. 5a to be very beneficial to the efficiency at low flight Mach number where a two- to three-fold increase of the latter can be obtained. However, it does not increase significantly the efficiency at high Mach number. This is caused in part by less power being bypassed to the high-speed duct for increasing Mach number because a higher thrust can be obtained by adding momentum to the slower flow exiting the fuel cells. Moreover, this is caused partly by the higher kinetic energy of the incoming air at high Mach number reducing the dependence of the thrust on the mass flow rate.

Depicted in Fig. 5b, the efficiency is observed to be progressively more sensitive to the heat/work ratio in the fuel-cell duct rather than in the high-speed duct for increased flight Mach number. This trend originates partly from the increasing fraction of the power being bypassed to the fuel-cell duct as the Mach number is raised, hence leading to a more pronounced sensitivity of the efficiency to the losses occurring in that part of the engine. In addition, reducing the heat/work ratio in the fuel-cell duct helps minimize the losses in the generator, which can become substantial at high Mach number. Indeed, it is emphasized that the heat-addition processes can be regarded as losses because only a small portion of the heat can be converted to work because of the small amount of compression.

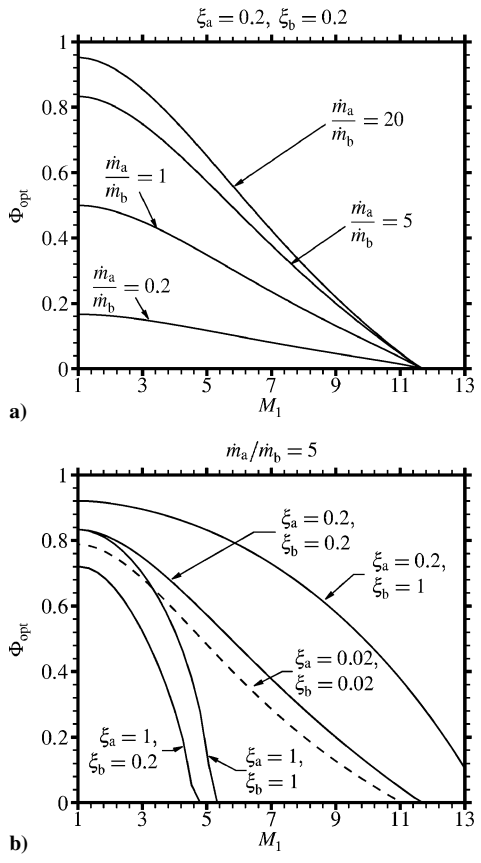

Fig. 4 Optimal power bypass ratio as a function of the Mach number.

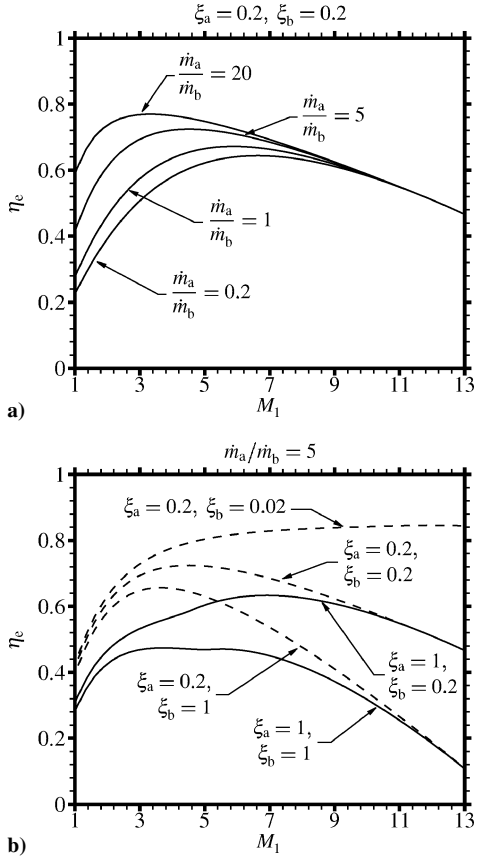

Fig. 5 Engine efficiency as a function of the flight Mach number.

Magnetic Field

In this section, the effect of the magnetic field strength on the heat/work ratio is assessed. Because the magnetic field is dependent on the conductivity, which itself influences the amount of heat deposited in the flow through external ionization, it is convenient at this stage to find a relationship between the ionization power and the conductivity. Electron beams are here chosen as the external ionizers as they are considered to be the less power-demanding approach to sustain an adequate level of electrical conductivity in low-temperature air.[15]

At steady state, assuming that the positive ion number density equals the electron number density and that the prevalent electron loss mechanisms are the dissociative recombination processes $e^- + O_2^+ \rightarrow O + O$ and $e^- + N_2^+ \rightarrow N + N$, the electron number density can be written as

$$n_e^2 = Q_i / k_{\mathrm{dr}} Y_i \tag{28}$$

where Q_i is the ionization power per unit volume and the energy cost of an ion-electron pair Y_i can be taken as 35 eV, which is only 2–3 times the energy required to ionize air molecules.[16] Taken from the Kossyi et al. kinetic scheme for nonequilibrium discharges in cold air,[17] the rate constant of dissociative recombination k_{dr} is set to 10^{-13} m^3/s assuming an electron temperature of 1200 K.

Equation (28) does not take into account electron loss mechanisms other than those caused by dissociative recombination. For instance, electrons could also be lost through dissociative attachment reactions such as $e^- + O_2 + 3.6\ \mathrm{eV} \rightarrow O + O^-$ or through third-body electron attachment processes of the form $e^- + O_2 + M \rightarrow O_2^- + M$. Although dissociative attachment is probably insignificant and electron attachment could be balanced by detachment for low-temperature air at high Mach number,[16] such reactions are dependent on the magnitude of the electric field as well as on the electron temperature, which could vary significantly throughout the flight Mach-number envelope of the magjet. Being outside the scope of this paper, future studies are needed to substantiate the impact of the inflow conditions and of the ionization power on the different electron loss mechanisms.

Following the approach outlined in Chapter 6 in Ref. 18, an expression relating the effective conductivity to the electron number density for a weakly ionized gas can be shown to correspond to

$$\sigma_e = \frac{e^2 n_e}{m_e n_n k_c \left(1 + \beta_e' \beta_i' \boldsymbol{B}_z^2 / \rho^2\right)} \tag{29}$$

where the concentration of neutral components can be taken as $n_n = \rho \mathcal{A} / \mathcal{M}_a$ and where the electron scattering rate constant k_c is set to 2×10^{-14} m^3/s as suggested in Ref. 19.

The ionization power Q_i can then be written in terms of the magnetic field and the heat/work ratio through Eq. (8) noting that the current corresponds to $\sigma_e q \boldsymbol{B}_z (k-1)$ through Ohm's law. Then, combining Eqs. (28) and (29) and substituting the effective conductivity into Eq. (13) gives the following relationship between the magnetic field and the Mach number:

$$\frac{(\xi - k + 1)(k-1)^2}{\left[1 + \beta_e' \beta_i' \left(\boldsymbol{B}_z^2 / \rho^2\right)\right]^2} \frac{\boldsymbol{B}_z^4}{\rho^4} (x_2 - x_1) \rho q = \frac{m_e^2 \mathcal{A}^2 k_c^2 Y_i k_{\mathrm{dr}}}{\mathcal{M}_a^2 e^4} \frac{b\gamma + 1}{b(\gamma + 1)\gamma} \times \ell_n \left\{ \left[\frac{M_2^2 \left(b - M_1^2\right)}{M_1^2 \left(b - M_2^2\right)} \right]^{(b-1)/b} \frac{\exp\left(M_2^{-2}\right)}{\exp\left(M_1^{-2}\right)} \right\} \tag{30}$$

To yield the smallest ratio of $\boldsymbol{B}_z / \rho$ for a given heat/work ratio and Mach-number change, the load factor k is such that one-third of the heat originates from ionization and two-thirds from Joule heating:

$$k = \tfrac{2}{3} \xi + 1 \tag{31}$$

which is obtained by setting to zero the partial derivative of the left-hand side of Eq. (30) with respect to k. Equation (30) holds true in a constant-area duct as long as $\boldsymbol{B}_z / \rho$, ξ, γ, and k are constant along the integration path.

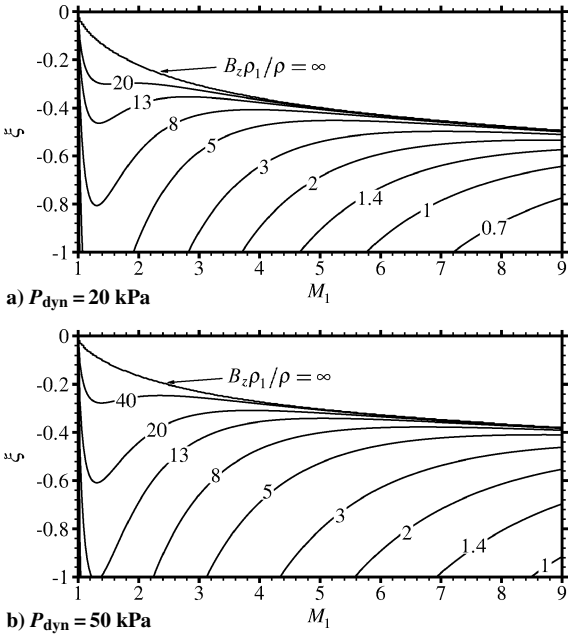

Fig. 6 Magnetic field in the energy extraction section (Teslas).

Energy Extraction

Noting that ρq remains constant in the constant-area energy extraction section, that the dynamic pressure corresponds to $\rho_1 q_1^2 / 2 = \rho_1 q_1 M_1 a_1 / 2$, and that the Mach number at the entrance of the fuel cells is fixed to 1, Eq. (30) can yield $\boldsymbol{B}_z / \rho$ should ξ, γ, the generator length, and the flight Mach number be given.

The magnetic field strength is plotted in Figs. 6a and 6b for a dynamic pressure of 20 and 50 kPa, respectively. The incoming air sound speed is set to 313.2 m/s, and the length of the generator is set to 5 m. The assumption of a constant sound speed is good in this case as the air temperature does not vary much throughout the atmosphere.[20]

The lower magnetic field associated with a high flight Mach number is postulated to be caused primarily by the decrease in flow density as the Mach number is increased. A lower flow density would require a lower magnitude of the magnetic field for primarily two reasons: 1) because the electromagnetic force acts on the flow on a volume rather than mass basis, the density decrease induces a considerable reduction in the magnetic field; and 2) a lower amount of power needs to be diverted to the electron beam ionizers to attain a given conductivity for lower flow density. The impact of the flow density can also be seen through the effect of the flight dynamic pressure: as the latter increases the density also increases, which leads to a higher magnetic field strength.

Interestingly, there exists a limit in the reduction of the heat/work ratio at a given Mach number, independently of the magnetic field strength. This phenomenon, related to the Hall and ion slip effects, can be explained as follows. To reduce the heat/work ratio, it is necessary to increase the Stuart number with the latter being proportional to the product between the effective conductivity and the square of the magnetic field. When the Hall parameter reaches high values (either as a result of a high magnetic field or a low flow density), the effective conductivity varies inversely proportional to the square of the magnetic field. Therefore, because of the Hall and ion slip effects the Stuart number would reach a finite value even in the limit of an infinite magnetic field, hence limiting the reduction of the heat/work ratio.

Momentum Addition

The magnetic field in the momentum addition sections can be determined similarly to the one in the energy extraction section. However, the Mach number at stations 2*a* and 4*b* is not user specified but must rather be found through Eqs. (20) and (22).

The magnetic field is plotted in Fig. 7 for an incoming sound speed of 313.2 m/s, a mass-flow-rate ratio of 5, a flight dynamic

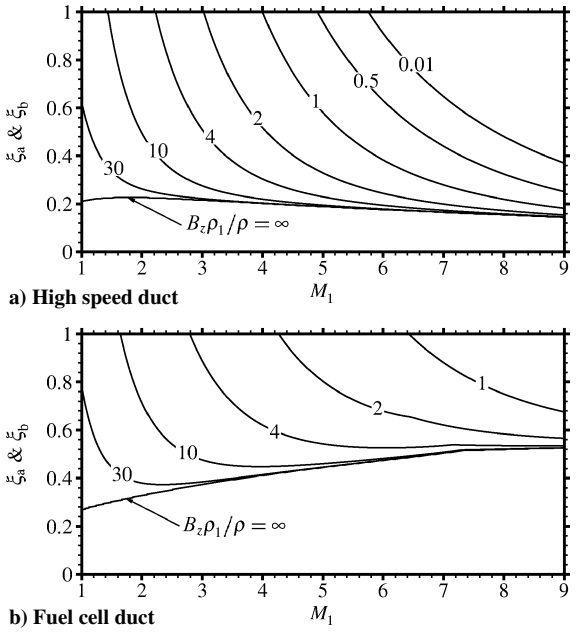

Fig. 7 Magnetic field in the momentum addition sections (Teslas); the flight dynamic pressure is of 20 kPa.

pressure of 20 kPa, a fuel specific energy of 142 MJ/kg, and with the length of the momentum addition sections in the high-speed and fuel-cell ducts fixed to 10 m and 5 m, respectively. Also, the Mach-number, stagnation-pressure, and stagnation-temperature ratios between stations 3*b* and 4*b* are set to unity.

Both in the fuel-cell and high-speed ducts, a pronounced influence of the flight Mach number on the magnetic field can be observed with a 15- to 60-fold reduction of the latter from Mach 1 to 7. This is attributed primarily to two effects: 1) not as much power is needed to ionize lower density flow to a certain conductivity; 2) because the Lorentz force acts on a volume basis rather than a mass basis, not as high of a magnetic field strength is required for lower density flow. Additionally, as was observed in Fig. 4, the amount of power bypassed to the high-speed duct diminishes as the flight Mach number increases, hence resulting in a further decrease of the magnetic field in that part of the engine.

Although not shown here, an increase of the flight dynamic pressure results in a similar magnetic field increase as in the energy extraction section because of the greater amount of power necessary to ionize higher density flow.

Specific Impulse

The specific impulse is defined here as the ratio between the engine thrust and the fuel mass flow rate times the gravitational acceleration, that is, $I_{sp} \equiv F/\dot{m}_{fuel}g$. Noting that $\dot{m}_{fuel} = \dot{m}_b\phi_s$, the specific impulse takes the following form:

$$I_{sp} = \frac{F}{\dot{m}_b\phi_s g} = \frac{Fq_1\mathcal{P}_2}{q_1\mathcal{P}_2\dot{m}_b\phi_s g} = \frac{\mathcal{P}_2}{\dot{m}_b q_1^2}\frac{\eta_e q_1}{\phi_s g} = \frac{\eta_{fc}e_f}{a_1 g}\frac{\eta_e}{M_1} \tag{32}$$

where $\mathcal{P}_2$ is taken from Eq. (24) and where the heat/work ratios in the different parts of the engine are determined iteratively from Eq. (30) with $\boldsymbol{B}_z\rho_1/\rho$ and the length of the MPD energy addition/extraction devices fixed. This results in a different value of the heat/work ratio in the high-speed duct as well as in the energy extraction/addition sections of the fuel-cell duct. The specific impulse is hence seen to be a function of the following parameters:

$$I_{sp} = f_3\left[\gamma, \frac{\phi_s\eta_{fc}e_f}{a_1^2}, \frac{\eta_{fc}e_f}{a_1 g}, M_{2b}, M_{3b}, \frac{P_{3b}^\circ}{P_{2b}^\circ}, \frac{T_{3b}^\circ}{T_{2b}^\circ}, M_1, a_1, P_{dyn}, \right.$$

$$\left.\frac{\boldsymbol{B}_z}{\rho}\rho_1, (x_{2a}-x_{1a}), (x_{2b}-x_{1b}), (x_{4b}-x_{3b}), \frac{\dot{m}_a}{\dot{m}_b}\right] \tag{33}$$

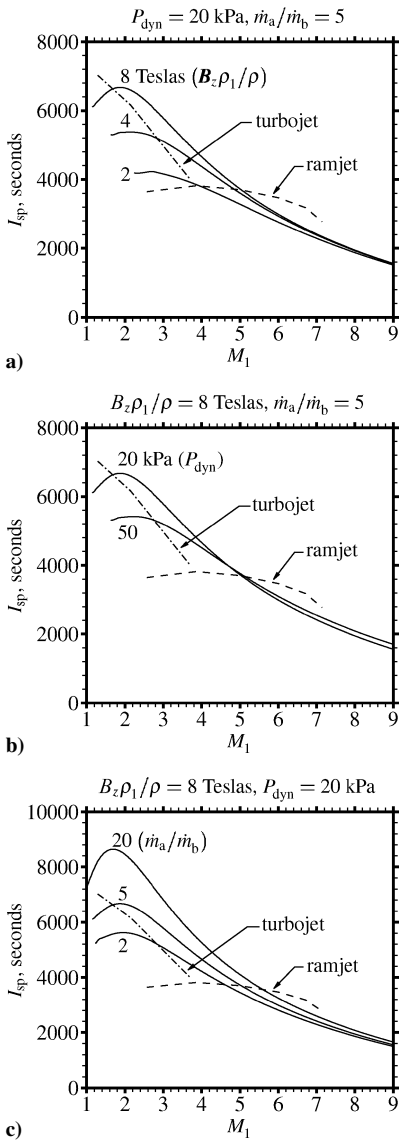

Fig. 8 Specific impulse vs the flight Mach number; all engines use hydrogen as fuel.

where the Mach number at stations 2*b* and 3*b* as well as the stagnation-pressure/temperature ratios across the fuel-cell compartment are set to 1. Also, the fuel-cell efficiency is fixed to 0.6, the incoming sound speed to 313.2 m/s, the fuel specific energy to 142 MJ/kg, the high-speed duct energy addition section length to 10 m, and the length of the energy extraction/addition sections in the fuel-cell duct to 5 m.

The magjet specific impulse is plotted in Fig. 8 and compared to the one of a turbojet and ramjet over their respective range of operation. For a magnetic field strength of 8 T, mass flow rate ratio of 5, and flight dynamic pressure of 20 kPa, the specific impulse of the magjet is seen to be at least equal and up to 30% times higher than the one of conventional engines throughout the Mach number range 1.6–5. Even for a four-fold reduction in the magnetic field, the magjet would still yield a specific impulse as high as the one of the conventional engines at a Mach number of 4. This somewhat small impact of the magnetic field on the magjet performance at high Mach number is related to the Hall and ion slip effects: for flight along a constant dynamic pressure path, the decrease in flow density associated with higher flight speed entails very high Hall parameters, which effectively prevent a reduction of the heat/work ratio through a raise in the magnetic field.

Although the Hall and ion slip effects have a small impact on the performance at low flight Mach number because of the high flow density, the performance is there hampered by the higher energy

required to ionize the flow. As attested in Fig. 8a, a magnetic field strength in excess of 8 T is necessary to match the performance of the turbojet for a Mach number less than 1.6. Another difficulty facing the magjet in the low-Mach-number range is the choking that would occur in the high-speed duct as a result of the significant heat addition through ionization and Joule heating. This problem could be overcome through a rise of the magnetic field, a rise in the mass flow rate ratio, or a decrease in the flight dynamic pressure. Alternately, the high-speed duct could be designed to allow bleeding to prevent choking.

As can be observed in Fig. 8c, a change in the mass flow ratio does not affect significantly the specific impulse at high Mach number. This is partly caused by a smaller amount of power being bypassed to the high-speed duct, but this is also caused by the higher kinetic energy of the incoming air. Indeed, a high-mass-flow-rate ratio improves the engine efficiency considerably only when the power added induces a high change in the flow speed, which is not the case when the air kinetic energy is very high. On the other hand, a 10-fold increase in the mass flow ratio can yield substantial gains in specific impulse when the incoming air kinetic energy is lower, with as much as a 60% increase observed at Mach 2.

Gains and Losses Through Fuel Cells

By maintaining the flow Mach number less or equal to one at the fuel-cell compartment entrance through the use of a MPD generator, no losses as a result of shock waves would occur through the fuel cells. Nonetheless, some losses in stagnation pressure could still be present because of skin friction or other phenomena. However, even for a somewhat considerable stagnation pressure loss through the fuel cells, the engine performance is seen not to be affected too considerably at least up to a Mach number of 6. For instance, using a mass flow rate ratio of 5, a dynamic pressure of 20 kPa, engine length of 10 m, and a magnetic field strength of 8 T, the decrease in specific impulse would be of only 7–13% in the Mach number range 2–6 should the stagnation pressure decrease two-fold.Even for a four-fold decrease in the stagnation pressure, the specific impulse is seen not to decrease by more than 30% in the same Mach-number range.

Further, these losses could be offset by the gains in thrust that would occur should the excess heat generated by the fuel cells be dissipated to the airflow. This can be assessed with the help of Eq. (25), which would yield the stagnation temperature across the fuel cells for a given value of $\mathcal{P}_5$. Assuming a constant-pressure heat-addition process, the stagnation-pressure ratio would vary according to[12]

$$\frac{P^{\circ}_{3b}}{P^{\circ}_{2b}} = \left(\frac{T_{2b}/T_{1b} + \left\{ 2(\gamma-1)M^2_{1b} \Big/ \left[2 + (\gamma-1)M^2_{2b} \right] \right\} \left(\mathcal{P}_5 \Big/ \dot{m}_b q^2_{1b} \right)}{T_{2b}/T_{1b} + (\gamma-1)M^2_{1b} \left(\mathcal{P}_5 \Big/ \dot{m}_b q^2_{1b} \right)} \right)^{\gamma/(\gamma-1)} \tag{34}$$

where T_{2b}/T_{1b} can be found from Eq. (12). For a mass flow rate ratio of 5, a magnetic field of 8 T, a dynamic pressure of 20 kPa, and $\mathcal{P}_5 = 0.4\mathcal{P}_2$, the effect of heat addition by the fuel cells is seen to translate into a 12% increase in thrust at Mach 2. When the Mach number is raised to 6, the increase in thrust is more considerable at 29%. This is because of the more substantial compression through the MPD generator at higher Mach number, hence resulting in a greater amount of heat being converted to work, and hence thrust.

Conclusions

A fuel-cell-powered magnetoplasma jet engine (magjet) using electron-beam ionization is here proposed as a substitute to the turbojet and ramjet for flight up to hypervelocities. Over conventional engines, the magjet is advantaged by 1) a single engine design to reach hypersonic velocities, 2) the lack of a brittle and hard-to-cool variable geometry inlet, 3) the use of fuel cells yielding less emissions, and 4) a possible higher air bypass ratio increasing the efficiency and reducing the noise level.

Although the magjet has the potential to yield a specific impulse equal or greater than the one of the turbojet or ramjet for flight up to hypervelocities, there are some aspects of the engine that require special attention and further study.

A high-mass-flow-rate ratio is found to be important to the performance especially at lower Mach number. However, such a performance gain would necessarily be accompanied by a greater engine cross-sectional area, which could lead to performance penalties such as increased engine mass and skin friction. Further studies are required to assess the impact of the mass flow rate ratio on the skin friction as well as on the mass of the magnet, ionizers, and additional equipment necessary to convert the low-voltage fuel-cell power output to the high-voltage power input needed by the electron-beam ionizers.

To prevent excessive heat loads and shocks from occurring in the fuel-cell compartment at high speed, it is necessary to reduce the incoming air Mach number and stagnation temperature by extracting sufficient enthalpy through a magnetoplasmadynamic (MPD) generator. In this way, the stagnation temperature can be kept within five times the freestream temperature for a flight Mach number less than six. At higher speeds however, the electron-beam power requirements and the ion slip effect prevent the stagnation temperature to be decreased to that level, independently of the magnetic field strength. Substantial cooling of the fuel cells would hence be required at hypervelocities. Furthermore, reducing the flow Mach number to unity from hypersonic values using a constant-area MPD generator could be particularly challenging to achieve because of the possibility of boundary-layer separation and flow instabilities.

The magnetic field is seen to affect substantially the engine performance especially at low Mach number where the ionization power requirements are high and the Hall parameter is relatively low. For a flight dynamic pressure fixed to 20 kPa, a specific impulse within 15% of the one of the turbojet can be obtained in the flight Mach-number range 1–3 using a magnetic field of 8 T. From Mach 3 to 5, a magnetic field strength varying between 2 and 4 T would be sufficient. Although this is an encouraging value, it would nonetheless entail a Hall parameter varying between 5 and 30 for the flow conditions here considered. This could entail arcing between electrodes, large streamwise currents, or other difficulties requiring further investigation.

Acknowledgments

This work has been supported by the Brain Korea 21 Project in 2003–2004 and by the Natural Sciences and Engineering Research Council of Canada. The authors are thankful to the reviewers for their constructive comments that helped improve the quality of the manuscript.

References

[1]Gurijanov, E. P., and Harsha, P. T., "AJAX: New Directions in Hypersonic Technology," AIAA Paper 96-4609, 1996.

[2]Kopchenov, V., Vatazhin, A., and Gouskov, O., "Estimation of Possibility of Use of MHD Control in Scramjet," AIAA Paper 99-4971, 1999.

[3]Lee, Y.-M., Czysz, P. A., and Petley, D., "Magnetohydrodynamic Energy Bypass Applications for Single Stage-to-Orbit Vehicles," AIAA Paper 2001-1901, 2001.

[4]Brichkin, D. I., Kuranov, A. L., and Sheikin, E. G., "Scramjet with MHD Control Under 'AJAX' Concept. Physical Limitations," AIAA Paper 2001-0381, 2001.

[5]Litchford, R. J., Cole, J. W., Bityurin, V. A., and Lineberry, J. T., "Thermodynamic Cycle Analysis of Magnetohydrodynamic-Bypass Hypersonic Airbreathing Engines," *Journal of Propulsion and Power*, Vol. 17, No. 2, 2001, pp. 477–480.

[6]Poggie, J., "Numerical Simulation of Electromagnetic Flow Control for Hypersonic Systems," AIAA Paper 2002-5182, Sept. 2002.

[7]Bottini, H., Bruno, C., and Czysz, P. A., "Is the MHD Scramjet Really an Advantage," AIAA Paper 2003-5046, July 2003.

[8]Scott, T., Riggins, D. W., and Christensen, K., "Thermodynamic Analysis of the Transposed-Cycle," AIAA Paper 2001-3748, July 2001.

[9]Song, C., "Fuel Processing for Low-Temperature and High-Temperature Fuel Cells. Challenges, and Opportunities for Sustainable Development in the 21st Century," *Catalysis Today*, Vol. 77, No. 1, 2002, pp. 17–49.

[10]Folkesson, A., Andersson, C., Alvfors, P., Alakula, M., and Overgaard, L., "Real Life Testing of a Hybrid PEM Fuel Cell Bus," *Journal of Power Sources*, Vol. 118, No. 2, 2003, pp. 349–357.

[11]Godat, J., and Marechal, F., "Optimization of a Fuel Cell System Using Process Integration Techniques," *Journal of Power Sources*, Vol. 118, No. 2, 2003, pp. 411–423.

[12]Parent, B., and Jeung, I.-S., "Quasi One-Dimensional Performance Analysis of a Magnetoplasma Jet Engine," AIAA Paper 2004-3766, July 2004.

[13]Scott, T., and Riggins, D. W., "Work Interaction in Quasi-One-Dimensional Flows," *Journal of Propulsion and Power*, Vol. 16, No. 6, 2000, pp. 1053–1059.

[14]Aubrecht, G., *Energy*, 2nd ed., Prentice–Hall, Upper Saddle River, NJ, 1995.

[15]Macheret, S. O., Shneider, M. N., and Miles, R. B., "Magnetohydrodynamic Power Extraction from Cold Hypersonic Airflows with External Ionizers," *Journal of Propulsion and Power*, Vol. 18, No. 2, 2002, pp. 424–431.

[16]Macheret, S. O., Shneider, M. N., and Miles, R. B., "Electron-Beam-Generated Plasmas in Hypersonic Magnetohydrodynamic Channels," *AIAA Journal*, Vol. 39, No. 6, 2001, pp. 1127–1138.

[17]Kossyi, A., Kostinsky, A. Y., Matveyev, A. A., and Silakov, V. P., "Kinetic Scheme of the Non-Equilibrium Discharge in Nitrogen-Oxygen Mixtures," *Plasma Sources Science and Technology*, Vol. 1, No. 3, 1992, pp. 207–220.

[18]Cowling, T. G., *Magnetohydrodynamics*, Interscience, New York, 1956.

[19]Brichkin, D. I., Kuranov, A. L., and Sheikin, E. G., "The Potentialities of MHD Control for Improving Scramjet Performance," AIAA Paper 99-4969, 1999.

[20]*The U.S. Standard Atmosphere (1962)*, U.S. Government Printing Office, Washington, D.C., 1962.